

# Spin squeezing enhanced dual species atom interferometric accelerometer employing large momentum transfer for precision test of the equivalence principle

Jinyang Li<sup>1</sup>, Gregório R. M. da Silva<sup>1</sup>, Schuyler Kain<sup>1</sup>, Jason Bonacum<sup>3</sup>, David D. Smith<sup>4</sup>, Timothy Kovachy<sup>1</sup>, and Selim M. Shahriar<sup>2,3</sup>

<sup>1</sup> Department of Physics and Astronomy, Northwestern University, Evanston, IL 60208, USA

<sup>2</sup> Department of Electrical and Computer Engineering, Northwestern University, Evanston, IL 60208, USA

<sup>3</sup> Digital Optics Technologies, Rolling Meadows, IL 60008, USA

<sup>4</sup>NASA Marshall Space Flight Center, Space Systems Department, ES23, Huntsville, Alabama 35812, USA

## Abstract

We theoretically prove the feasibility of applying spin squeezing to a light pulse atom interferometer even in the presence of large momentum transfer using off-resonant Raman transitions, in order to enhance the sensitivity of accelerometry close to the Heisenberg limit. We also show how to implement this scheme in a dual-species atom interferometer for precision test of the equivalence principle by measuring the Eötvös parameter, and identify the spin squeezing protocol that is best suited for such an experiment. For a space borne platform in low earth orbit, such a scheme may enable the measurement of the Eotvos parameter with a sensitivity of the order of  $10^{-20}$ .

## 1. Introduction

The dual-species light pulse atom interferometer offers the potential to test the equivalence principle [1, 2, 3, 4, 5, 6, 7, 8, 9, 10] and to search for the wavelike dark matter [11, 12] with high precision. Enhancing the sensitivity of a dual species atom interferometer with the technique of large momentum transfer (LMT) [13, 14, 15, 16] has been demonstrated [1, 2]. However, another

technique that can in principle enhance the sensitivity of the atom interferometer, namely spin squeezing [17, 18, 19, 20, 21], has not yet been applied to any type of atom interferometer. In recent years, we have been investigating, separately, the use of LMT in atom interferometry [13] as well as the application of various protocols using one-axis-twist squeezing (OATS) for enhancing the sensitivity of atomic interferometers and atomic clocks [22, 23, 24]. Arguably the most promising approach for applying OATS to atomic interferometry makes use of the so-called generalized echo squeezing protocol (GESP) [22], which is predicted to yield a sensitivity of the Heisenberg limit within a factor of  $\sqrt{2}$ . Other protocols of interest with similar degree of enhancement in sensitivity include the Schrödinger cat state protocol (SCSP) [23, 24], and the conventional echo squeezing protocol (CESP) [25, 26].

Each of the squeezing protocols mentioned above employs the squeezing operation and the inverse-squeezing (echo) operation. Both acceleration and rotation can induce a phase shift in the interferometer. For rotation sensing employing these protocols, the phase shift is accumulated in the two dark periods [13, 22]. Therefore, as long as the squeezing operation is implemented before the first dark period and the inverse-squeezing is implemented after the second dark period, the phase shift will be accumulated on the squeezed state. However, for acceleration sensing, the phase shift depends on the relative phases of the second and third pulses with respect to that of the first pulse. It is also important to note that in these protocols the first pulse is applied before the squeezing operation and the third pulse is applied after the inverse-squeezing operation. In addition, these protocols also contain many auxiliary  $\pi/2$  pulses, and the relative phases of these pulses with respect to that of the first pulse will also contribute to the net phase shift produced by acceleration. Accordingly, a careful analysis is needed to determine what the effective phase shift

would be due to acceleration under each of these protocols, and whether the protocols themselves need be modified for optimal accelerometry.

In addition, it is not obvious whether the squeezing protocols mentioned above are compatible with LMT so that spin squeezing can enhance the sensitivity of an atom interferometer that already employs LMT, especially a dual-species atom interferometer. For LMT, the most widely used techniques are sequential Bragg transitions (SBT) [2, 16] and sequential Raman transitions (SRT) [13, 14, 15]. To date, the best experimental results, especially in the context of dual species atom interferometry, has been obtained using the application of SBT [16]. In principle, two momentum states with the same internal state produced by a Bragg transition can also be squeezed [27]. However, squeezing the momentum states may not work for Rb, mainly due to its wide transition linewidth. Besides, a narrow linewidth of the squeezing light is also required for squeezing the momentum states. For the SRT, although this technique overcomes this problem, it is still not obvious whether this technique of LMT is compatible with the squeezing protocols mentioned above. Furthermore, for a dual-species atom interferometer, one immediate problem that can be seen for incorporating OATS into LMT is that for the cavity-assisted OATS, generally the optical cavity used for spin squeezing needs to be tuned different frequencies for different species of atoms. In this paper we show that LMT with SRT is compatible with the spin squeezing protocols mentioned above and how to construct a scheme that incorporates these squeezing protocols into a dual-species atom interferometer.

The rest of the paper is organized as follows. In Section 2, we give the general mathematical description of an off-resonant Raman light pulse that is independent of the specific quantum state. In Section 3, we use the general way of describing the light pulses to analyze the signal of the atom interferometer employing both LMT and OATS. In Section 4, we propose the scheme of a dual-

species atom interferometer employing both LMT and OATS that can be used for the equivalence principle test. Concluding remarks are made in Section 5.

## 2. Generalized Model for Off-Resonant Raman Light Pulses

We first introduce the notations necessary for describing the off-resonant Raman light pulses. Each atom is modeled as a three-level system with the two ground states denoted as  $|\uparrow\rangle$  and  $|\downarrow\rangle$ , and the excited state denoted as  $|e\rangle$ . In practice, the two ground states are typically the  $m_F = 0$  Zeeman substates of the two hyperfine ground states of an alkali atom. The Raman beam coupling the two states  $|\uparrow(\downarrow)\rangle$  and  $|e\rangle$  is denoted as  $\mathbf{k}_{\uparrow(\downarrow)}$ . This three-level system can be reduced to a two-level system, with the effective wavenumber of the pair of counter-propagating Raman beams expressed as  $\mathbf{k}_{\text{eff}} = (\mathbf{k}_\uparrow - \mathbf{k}_\downarrow)$  if the direction of  $\mathbf{k}_{\text{eff}}$  is defined to be that of  $\mathbf{k}_\uparrow$ . The absolute value of the effective wavenumber can be expressed as  $k_{\text{eff}} = (k_\uparrow + k_\downarrow) \approx 2k_{\uparrow(\downarrow)}$ , where  $k_{\uparrow(\downarrow)}$  is the absolute value of the corresponding wavenumber. The two-level system can be modeled as spin-1/2 pseudo-spinors, with the spin operator defined as  $\mathbf{s} = (s_x, s_y, s_z)$ . In this notation, the subscripts  $\{x, y, z\}$  represent the three dimensions of the Bloch sphere. The effective Hamiltonian in the absence of two-photon detuning can be expressed as

$$H = \frac{1}{2} \begin{bmatrix} 0 & \Omega e^{-i\phi} \\ \Omega e^{i\phi} & 0 \end{bmatrix} \quad (1)$$

where  $\phi = \mathbf{k}_{\text{eff}} \cdot \mathbf{r}$  is the initial phase (which is time-independent) of the light field at the position of the atom. The corresponding propagators for generalized  $\pi/2$  and  $\pi$  pulses can be expressed as:

$$U_{\pi/2} = \frac{1}{\sqrt{2}} \begin{bmatrix} 1 & -ie^{-i\phi} \\ -ie^{i\phi} & 1 \end{bmatrix} = e^{-i\phi s_z} e^{-i(\pi/2)s_x} e^{i\phi s_z} \quad (2)$$

$$U_{\pi} = \begin{bmatrix} 0 & -ie^{-i\phi} \\ -ie^{i\phi} & 0 \end{bmatrix} = e^{-i2\phi s_z} e^{-i\pi s_x} = e^{-i\pi s_x} e^{i2\phi s_z} \quad (3)$$

where  $\phi = 0$  corresponds to the pulses that represent rotations around the  $x$  axis. It should be noted that these propagators only contains the linear terms of the spin operators in the exponent, so that the corresponding propagators for the ensemble can be obtained simply by replacing the single atom operators  $s_w$  ( $w = x, y, z$ ) with the operators  $S_w$ , where  $S_w$  is the sum of the single atom operators  $s_w$  of all the atoms.

### 3. Analysis of the spin squeezing protocols for acceleration sensing

The three OATS based protocols mentioned earlier, namely the SCSP, the GESP and the CESP, all involve very similar sequences of pulses [22]. The differences are only the rotation axes of the  $\pi/2$  pulses and the duration of the squeezing and unsqueezing pulses. As such, we have shown these sequences in a unified manner in Figure 1, augmented to allow for extra pulses used to cause large momentum transfer (LMT). For concreteness, we first focus on the GESP that is optimal for the even parity of the number of atoms, denoted as GESP-e [22], in which all the  $\pi/2$  pulses are around the same axis. Without loss of generality, we assume that all the  $\pi/2$  pulses are around the  $x$  axis. For LMT, the case shown in Figure 1 uses sequential Raman transitions [13, 14, 15] with two additional  $\pi$  pulses in the beam splitter period ( $A_1$ ,  $A_2$ ,  $C_{-2}$  and  $C_{-1}$ ), and four additional  $\pi$  pulses ( $B_{-2}$ ,  $B_{-1}$ ,  $B_1$  and  $B_2$ ) in the reflection period, which yield a momentum transfer of  $5\hbar k_{\text{eff}}$ . For the general case, there can be  $n$  additional  $\pi$  pulses in the two beam splitter periods, and  $2n$  additional  $\pi$  pulses in the reflection period, giving a momentum transfer of  $(2n+1)\hbar k_{\text{eff}}$ . The first

$\pi/2$  pulse in period  $A$  is labeled as  $A_0$ . The additional  $\pi$  pulses are labeled as  $A_1$  to  $A_n$ . The pulses in period  $B$  and  $C$  are labeled in a similar way as shown in Figure 1. The net propagator for two consecutive  $\pi$  pulses with oppositely directed Raman beams, for example, pulse  $A_1$  and  $A_2$ , is calculated to be

$$\left( e^{-i2\phi_{A_1}S_z} e^{-i\pi S_x} \right) \left( e^{-i\pi S_x} e^{i2\phi_{A_2}S_z} \right) = \pm e^{i2(\phi_{A_2} - \phi_{A_1})S_z} = \pm e^{i2k_{\text{eff}} \cdot (r_{A_1} + r_{A_2})S_z} \quad (4)$$

The last step accounts for the fact that propagation direction of pulse  $A_1$  is reversed with respect to that of  $A_0$  (and  $A_2$ ), such that its effective wavenumber is  $(-k_{\text{eff}})$ . The sign  $\pm$  is evaluated to be  $+(-)$  if the number of atoms is even (odd). However, this sign issue is irrelevant in this context. It can be seen from Eq. (4) that two consecutive  $\pi$  pulses is equivalent to a rotation around the  $z$  axis on the Bloch sphere. With this result, it is easy to see that the propagator of all the  $\pi$  pulses can be expressed as

$$e^{i2k_{\text{eff}} \cdot \left( \sum_{j=1}^n r_{A_j} - \sum_{j=-n}^n r_{B_j} + \sum_{j=-n}^{-1} r_{C_j} \right) S_z} e^{-i\pi S_x} \quad (5)$$

which is a rotation around  $z$  axis on the Bloch sphere and a  $\pi$  pulse. Here, we have assumed that there is no Sagnac effect induced phase shift due to rotation. The net propagator for the first three pulses ( $A_0$ , squeezing pulse, and the auxiliary  $\pi/2$  pulse) can be expressed as

$$\left( e^{-i\phi_{A_0}S_z} e^{-i(\pi/2)S_x} e^{i\phi_{A_0}S_z} \right) e^{-i\mu S_z^2} \left( e^{-i\phi_{A_0}S_z} e^{-i(\pi/2)S_x} e^{i\phi_{A_0}S_z} \right) = e^{-i\phi_{A_0}S_z} e^{-i(\pi/2)S_x} e^{-i\mu S_z^2} e^{-i(\pi/2)S_x} e^{i\phi_{A_0}S_z} \quad (6)$$

Here,  $\mu$  is the OATS squeezing parameter. It should be noted that the time interval between  $A_0$  and the auxiliary  $\pi/2$  pulse must be very small such that the physical distance between state  $|\uparrow\rangle$  and  $|\downarrow\rangle$  is still much smaller than the coherence length of the atoms. Otherwise, these two  $\pi/2$

pulses will split the atom state twice, resulting in four atomic paths. Similarly, the net propagator for the last three pulses can be expressed as:

$$e^{-i\phi_{C_0}S_z}e^{-i(\pi/2)S_x}e^{-i\mu S_z^2}e^{-i(\pi/2)S_x}e^{i\phi_{C_0}S_z} \quad (7)$$

Combining Eqs. (5), (6) and (7), we find the overall propagator for all the pulses in the protocol to be:

$$e^{-i\phi_{A_0}S_z}e^{-i(\pi/2)S_x}e^{-i\mu S_z^2}e^{-i(\pi/2)S_x}e^{i\mathbf{k}_{\text{eff}} \cdot \left[ \mathbf{r}_{A_0} + 2 \left( \sum_{j=1}^n \mathbf{r}_{A_j} - \sum_{j=-n}^n \mathbf{r}_{B_j} + \sum_{j=-n}^{-1} \mathbf{r}_{C_j} \right) + \mathbf{r}_{C_0} \right] S_z} e^{-i(3\pi/2)S_x}e^{i\mu S_z^2}e^{-i(\pi/2)S_x}e^{i\phi_{C_0}S_z} \quad (8)$$

It should be noted that a pulse described by the propagator  $e^{-i(\pi/2)S_x}f(S_z)e^{-i(3\pi/2)S_x}$  is equivalent to the process described by  $f(S_y)$ , where  $f$  is an arbitrary analytical function [22]. It should also be noted that the rotation around  $z$  axis on the Bloch sphere in the beginning and at the end does not affect the signal. Given these facts, the propagator given in Eq. (8) can be simplified as

$$e^{-i(\pi/2)S_x}e^{-i\mu S_z^2}e^{i\mathbf{k}_{\text{eff}} \cdot \left[ \mathbf{r}_{A_0} + \left( \sum_{j=1}^n \mathbf{r}_{A_j} - \sum_{j=-n}^n \mathbf{r}_{B_j} + \sum_{j=-n}^{-1} \mathbf{r}_{C_j} \right) + \mathbf{r}_{C_0} \right] S_y} e^{i\mu S_z^2}e^{-i(\pi/2)S_x} \quad (9)$$

which is identical to the simplified equivalent GESP-e protocol given in Fig. 3 of Ref. [22], if we equate the intermediate phase shift to  $\mathbf{r}_{A_0} + \left( \sum_{j=1}^n \mathbf{r}_{A_j} - \sum_{j=-n}^n \mathbf{r}_{B_j} + \sum_{j=-n}^{-1} \mathbf{r}_{C_j} \right) + \mathbf{r}_{C_0}$ . Note that this phase shift is also exactly the same as the phase shift of the light pulse atom interferometer with LMT induced by acceleration, which equals  $\mathbf{k}_{\text{eff}} \cdot \mathbf{a} \left[ (2n+1)T^2 - 2n(n+1)T\tau \right]$  where  $T$  is the half duration of the interferometer and  $\tau$  is the time interval between two consecutive pulses that are not separated by the dark periods[13], as indicated in Figure 1. For  $T \gg \tau$ , the acceleration phase shift can be approximated as  $(2n+1)\mathbf{k}_{\text{eff}} \cdot \mathbf{a}T^2$ .

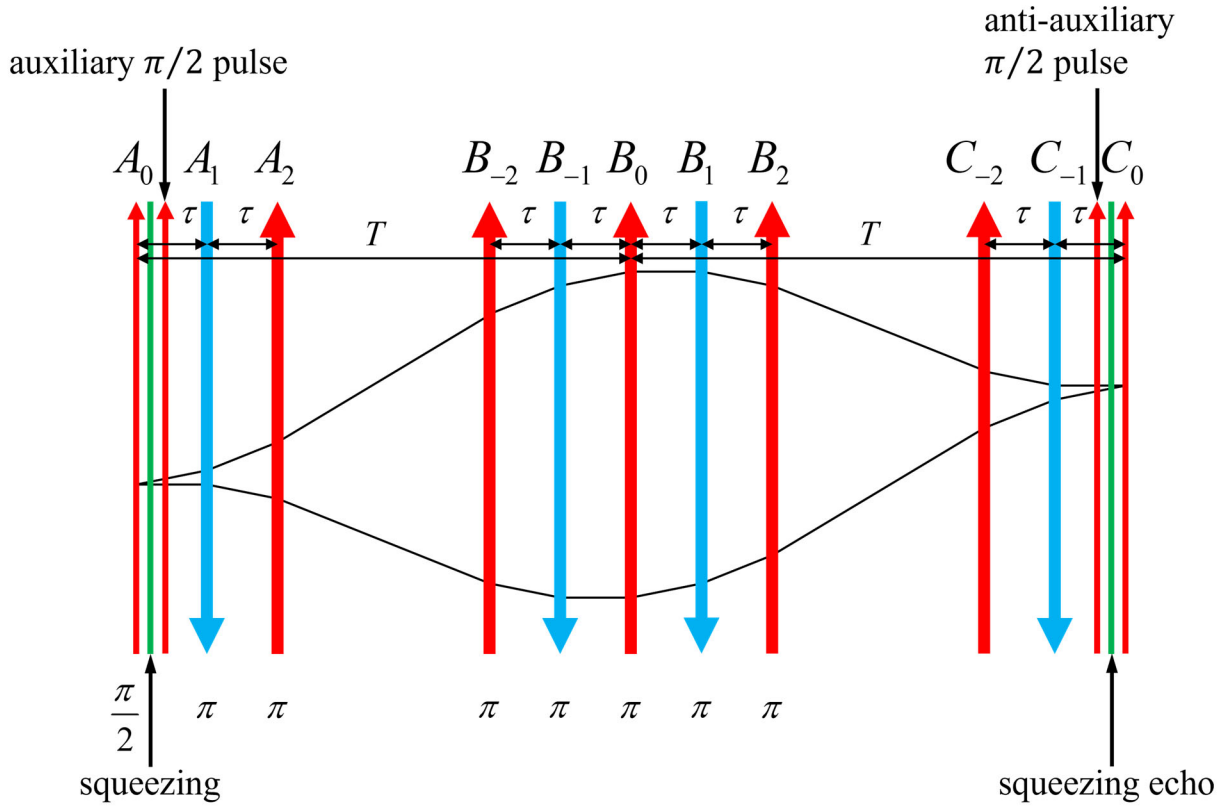


Figure 1 Example of the pulse sequence of the atom interferometer with spin squeezing and large momentum transfer. In this example, two  $\pi$  pulses in alternating directions are added in each atomic beam splitter period (i.e.,  $n = 2$ ), along with four additional  $\pi$  pulses in alternating directions in the reflection period, giving a momentum transfer of  $(2n + 1)\hbar k_{\text{eff}} = 5\hbar k_{\text{eff}}$ .

#### 4. Scheme for testing the equivalence principle

A dual-species atom interferometer can be used to test the equivalence principle [1, 2]. In such an interferometer, the two isotopes are initially captured in the same magneto-optic trap. So far, Bragg pulses have been used in dual-species atom interferometers employing  $^{87}\text{Rb}$  and  $^{85}\text{Rb}$  because a single pair of Bragg beams can address both isotopes. In this way, the effective wavenumber of the Bragg beams  $k_{\text{eff}}$  and the half duration of the interferometer protocol  $T$  are naturally the same for both isotopes. Therefore, the acceleration phase shift  $k_{\text{eff}}aT^2$  only depends on the acceleration  $a$  for both isotopes. In principle, Raman pulses can also be used for such a dual-species atom interferometer. However, two different pairs of monochromatic Raman beams (of course, we can

modulate a Raman beam to produce two frequency components) are needed to address these two isotopes. These two pairs of Raman beams can be combined so that their propagating directions are the same. To make the values of  $k_{\text{eff}}$  of the two pairs of Raman beams the same, we can produce them from the same laser. To produce the Raman beams for  $^{85}\text{Rb}$ , we guide a beam from that laser through an EOM tuned to  $\sim 1.5$  GHz, which is half the hyperfine splitting of the ground state. In this way, the +1 order and -1 order of the components differs by the hyperfine splitting and their average frequency is the laser frequency. Each of these frequency components can be extracted with a Fabry-Perot cavity. Alternatively, two different AOMs can be used for generating these frequency components, with one up-shifted and another down-shifted. Therefore, a pair of counter-propagating Raman beams for  $^{85}\text{Rb}$  can be prepared and their  $k_{\text{eff}}$  is exactly twice the laser frequency. If the Raman beams for  $^{87}\text{Rb}$  are prepared in the same way, their  $k_{\text{eff}}$  will also be twice the laser frequency, and thus equal the  $k_{\text{eff}}$  of the Raman beams for  $^{85}\text{Rb}$ . The frequencies of the Raman beams are schematically shown in Figure 2.

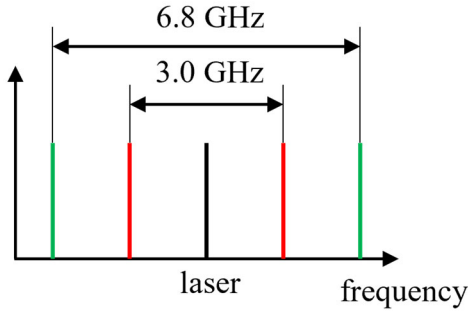


Figure 2 Schematic illustration of the frequencies of the Raman beams for  $^{85}\text{Rb}$  (red) and  $^{87}\text{Rb}$  (blue). The two frequencies of the Raman beams are generated with an EOM tuned to half the hyperfine splitting the ground state. Therefore, the average frequency of the two Raman beams is exactly the laser frequency.

OATS is realized via non-linear interaction between the atoms and the light in an optical cavity. A ring cavity is preferred because no standing wave will form, thus making the value of the single-photon Rabi frequency uniform longitudinally. The configuration of the apparatus is schematically

shown in Figure 4. In the model describing the mechanism of OATS, an atom is considered as a three-level system consisting of two ground states, denoted as  $|\uparrow\rangle$  and  $|\downarrow\rangle$ , and an excited state, denoted as  $|e\rangle$ . Ideally, to balance the light shifts of state  $|\uparrow\rangle$  and  $|\downarrow\rangle$ , the cavity should be tuned to the average frequency of the transitions from  $|\uparrow\rangle$  to  $|e\rangle$  and from  $|\downarrow\rangle$  to  $|e\rangle$  if we assume that the Rabi frequencies of these two transitions are the same. To address this issue, we assume first that the spin-up and spin-down states are, respectively, the  $F=2, m_F=0$  ( $F=1, m_F=0$ ) and  $F=3, m_F=0$  ( $F=2, m_F=0$ ) Zeeman sublevels for the case of  $^{85}\text{Rb}$  ( $^{87}\text{Rb}$ ). For these choices, if we ignore the energy differences among the hyperfine states within the excited state ( $5 P_{3/2}$ ) manifold, the Rabi frequencies of these two transitions will be the same for both isotopes, if the cavity mode is assumed to be right-circularly polarized, and the effective dipole matrix element for each leg is calculated as the root of the sum of the squares of the dipole matrix elements of the allowed transitions among the relevant Zeeman sublevels, as illustrated in Figure 3. Of course, to be more accurate, one must consider the energy differences among the hyperfine levels in the excited state manifold. Once these splittings are taken into account, it is easy to determine the required cavity resonant frequency that will perfectly balance the light shifts of state  $|\uparrow\rangle$  and  $|\downarrow\rangle$ , by adding up the light shifts due to each of the transitions shown in Figure 3, under the simplifying assumption that the detuning for each transition will be much larger than the Rabi frequencies due to the probe field. It should be noted, however, that while the use of balanced Rabi frequencies is assumed in all theoretical analyses of one axis twist squeezing using this approach, the balance between the light shifts is not an essential requirement. A deviation from this symmetric configuration will simply result in a linear term of  $S_z$  in the effective Hamiltonian apart from the squeezing term. In fact, another linear term exists even when symmetric light shifts are used. It can be shown that the

effects of these linear terms do not affect the enhancement in measurement sensitivity achievable using any variation of the OATS protocol, including the three mentioned earlier in this paper.

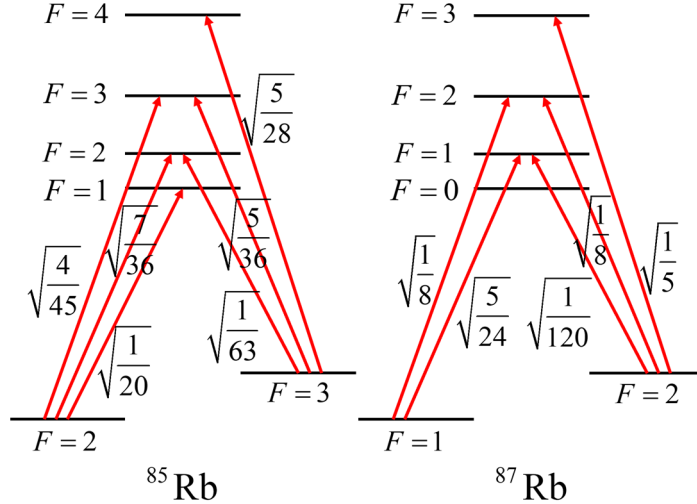


Figure 3 Relevant transitions for OATS. Here we have assumed that the spin-up and spin-down states are, respectively, the  $F=2, m_F=0$  ( $F=1, m_F=0$ ) and  $F=3, m_F=0$  ( $F=2, m_F=0$ ) Zeeman sublevels for the case of  $^{85}\text{Rb}$  ( $^{87}\text{Rb}$ ), and the cavity mode is right circularly polarized. If the energy differences among the hyperfine states within the excited state manifold are ignored, the light shifts are balanced because the sum of the squares of the dipole matrix elements of the allowed transitions on each leg is the same:  $4/45+7/36+1/20=5/28+5/36+1/63=1/3$  for  $^{85}\text{Rb}$  and  $1/8+5/25=1/120+1/8+1/5=1/3$  for  $^{87}\text{Rb}$ . Once these splittings are taken into account, it is easy to determine the required cavity resonant frequency that will perfectly balance the light shifts.

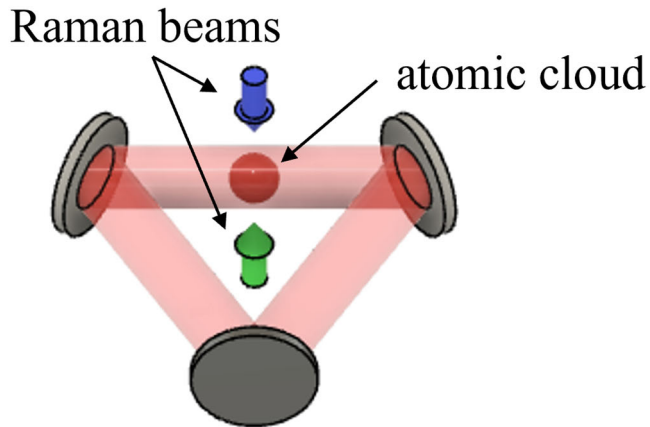


Figure 4 Schematic illustration of the configuration of the apparatus. The cavity is in the horizontal plane and the Raman beams are applied in the vertical direction.

Taking these factors into consideration, the same cavity can be used for squeezing both isotopes, although the cavity frequency cannot be optimized for both isotopes. However, if atoms

from both isotopes are present in the cavity simultaneously, the resulting non-linear interaction would produce a complex entangled among the atoms from both groups, instead of producing the ideal one axis twist squeezing interaction for each group. As such, the squeezing operations on these two isotopes must be carried out separately. Of course, if the two experiments were fully separated spatially, this requirement can be easily met. However, in order to suppress the common sources of noise, as well as minimize the required resources, which is a significant factor if this experiment is carried out in a space-borne platform, it is important to consider a geometry where both isotopes would be trapped using the same apparatus, and squeezed using the same optical cavity with the same cavity resonance frequency, which is possible based on the discussion presented above. As such, a key requirement is that the squeezing operation on the second isotope must not start until the first isotope atoms leave the cavity. Therefore, the sequence of operations depicted in Figure 1, for each isotope, has to be separated in time, by a duration  $\tau_D$ . In choosing the value of this delay time, it should be noted that the suppression of common mode noise would be cut off for frequencies larger than the inverse of this time delay,  $\tau_D^{-1}$ . Thus, the expected spectrum of sources of common mode noise, such as vibrations, would play a key role in choosing the value of this delay. Depending on whether the experiment is to be conducted terrestrially or on a space-borne platform in a low earth orbit, several approaches can be employed to meet this requirement of temporally separated operations, as described next.

Consider first the case where the experiment would be carried out terrestrially. In this case, the cavity would be placed slightly above the center of the magneto-optic trap (MOT). After the atoms are released from the MOT and cooled further, the cloud for one isotope would be launched first vertically as an atomic fountain. The mode diameter of the cavity would be designed to be large enough to ensure that the transit time for the atomic cloud across the cavity is large enough

to reach the desired value of the squeezing parameter:  $\mu \leq \pi/2$ . On the other hand, the transit time should also be short enough so that the first  $\pi/2$  pulse and the auxiliary  $\pi/2$  pulse do not split the atoms twice, as mentioned earlier. The first Raman pulse would be applied before the atoms enter the cavity, and the rest of the pulse sequence would follow the scheme depicted in Figure 1. The launching of the cloud of the second isotope would be delayed by  $\tau_D$ , chosen to be larger than the transit time of the first cloud through the cavity mode. The start time for each of the pulses in the operating sequence for this cloud would also be delayed by the same amount of time.

Consider next the case where the experiment would be carried out in a space-borne platform in a low earth orbit. The sequence of operations would again formally be the same, with the exception that the launch velocity for the atomic clouds would be much smaller than what would be used in the terrestrial case. Furthermore, a matched second cavity, placed well above the first one, would be used for the inverse squeezing operation. The distance between the two cavities would be given by the product of the launch velocity and the total time interval between the squeezing and inverse-squeezing steps shown in Figure 1. The choice of this interval as well as the launch velocity,  $V_L$ , would be dictated by the available length of the apparatus, as well as the parameter  $n$  that characterized the degree of large momentum transfer employed. It should be noted that the spectral extent of sources of vibrational noise, for example, is expected to be limited to very low frequencies, thus enabling the use of a larger value of  $\tau_D$  and correspondingly smaller value of the launch velocity.

In general, the value of  $\mu$  for  $^{85}\text{Rb}$  will be somewhat different from that for  $^{87}\text{Rb}$  if the same cavity mode and the same probe field is used. The sensitivity of the spin squeezing protocols depends on the value of  $\mu$  and the number of atoms, which will be different for these two isotopes.

However, a very important aspect of the GESP protocol is that it has the essentially the same sensitivity for a wide range of  $\mu$  [22] and thus is best suited for such a dual-species interferometer.

By modulating the phase of any one of the  $\pi$  pulses, denoted as  $\phi_p$ , we can obtain the signal (namely, the difference between the population of  $|\uparrow\rangle$  state and the population of  $|\downarrow\rangle$  state) versus the phase shift. The total phase shift is  $(2n+1)k_{\text{eff}}aT^2 + \phi_p$ . Although the sensitivity can be made the same for these two isotopes, the widths of the fringes as a function of  $\phi_p$  depend on the value of  $\mu$  and the number of atoms. Assuming, for example, that the value of  $\mu$  would be larger for  $^{85}\text{Rb}$ , and the number of atoms trapped for  $^{85}\text{Rb}$  would be higher, the fringes for  $^{85}\text{Rb}$  would be narrower. If the equivalence principle holds, the central peaks, which correspond to the point where  $(2n+1)k_{\text{eff}}aT^2 + \phi_p = 0$ , will coincide, as shown in Figure 5. Therefore, we can lock  $\phi_p$  to the central peak (i.e.,  $\phi_p = -(2n+1)k_{\text{eff}}aT^2$ ) of one isotope and check whether the signal of the other isotope deviates from its central peak.

Ideally, the sensitivity of the GESP can be expressed as  $(2n+1)k_{\text{eff}}\Delta aT^2 = \sqrt{2}/N$ , where  $N$  is the number of atoms during the interrogation time. For  $n = 5$ ,  $T = 1$  s, and  $N = 10^8$ , which are close to the values of the parameters adopted in Ref. [2], the uncertainty of the acceleration per shot is calculated to be  $7.9 \times 10^{-14}$  m·s<sup>-2</sup>. If the experiment is implemented on the ground or in a low earth orbit, the gravitational acceleration is  $\sim 9.8$  m·s<sup>-2</sup>. Therefore, the relative precision that can be achieved is  $\Delta a/a = 8.0 \times 10^{-16}$  per shot, which is four orders of magnitude higher than the sensitivity reported in Ref. [2]. Of course, the reason for this enhancement is that the sensitivity without spin squeezing is at the standard quantum limit, while the sensitivity of the GESP is close to the Heisenberg limit. Therefore, the factor of enhancement of sensitivity is  $\sim \sqrt{N} = 10^4$ .

Furthermore, if the experiment is implemented on a space-borne platform in a low earth orbit, the value of  $T$  can be much larger. If  $T = 100$  s and  $10^6$  shots are implemented, a relative sensitivity on the order of  $10^{-20}$  may be achievable in principle, assuming that sources of excess noise can be suppressed sufficiently.

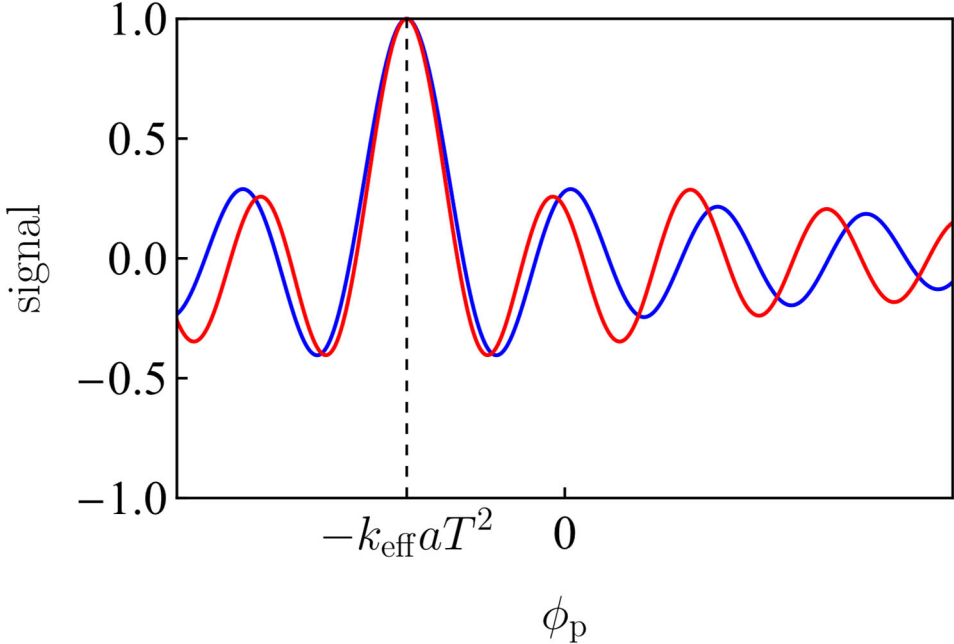


Figure 5 Example of the signals of the generalized echo squeezing protocol for  $^{85}\text{Rb}$  (red) and  $^{87}\text{Rb}$  (blue). The position of the central peak is at  $\phi_p = -k_{\text{eff}} a T^2$ . If the equivalence principle holds, the central peaks of both isotopes will coincide.

Both increasing the interrogation time and increasing the momentum transfer can enhance the sensitivity. However, for an experiment in the weightless environment, one must satisfy the constraint imposed by the length of the vacuum chamber,  $x$ , and the launch velocity,  $V_L$ :

$[(2n+1)\hbar k_{\text{eff}}/m + V_L]T \leq x$ . For simplicity of discussion, let us assume that  $V_L \ll (2n+1)\hbar k_{\text{eff}}/m$ . Recalling that the phase shift is  $\phi = (2n+1)k_{\text{eff}}aT^2$ , we find that

$\phi \leq \max T / \hbar$ , which is proportional to  $T$  but does not depend on  $n$ . Therefore, if the physical dimension of the apparatus is the primary constraint, it may be optimal to increase  $T$  at the expense of decreasing  $n$ , while satisfying the constraint  $[(2n+1)\hbar k_{\text{eff}}/m]T \leq x$ . However, other factors may restrict the maximum value of  $T$ , such as the expansion of the atomic cloud. Taking these factors into account, use of LMT corresponding to a non-zero value of  $n$  is expected to be useful for increasing the sensitivity of the experiment.

## 5. Conclusion

We have shown theoretically the feasibility of applying spin squeezing to a light pulse atom interferometer even in the presence of large momentum transfer using off-resonant Raman transitions, in order to enhance the sensitivity of accelerometry close to the Heisenberg limit. We also show how to implement this scheme in a dual-species atom interferometer for precision test of the equivalence principle by measuring the Eötvös parameter, defined as the ratio of the differential acceleration to the mean acceleration experienced by two objects with different inertial masses under free fall in a gravitational field. Based on experimental constraints, we find that the generalized echo squeezing protocol, which enhances the sensitivity close to the Heisenberg limit for a very broad range of values of the squeezing parameter, is the best suited for such an experiment. For a space borne platform in low earth orbit, such a scheme may enable the measurement of the Eotvos parameter with a sensitivity of the order of  $10^{-20}$ .

## Acknowledgement:

This work has been supported equally in parts by NASA grant number 80NSSC20C0161, the Department of Defense Center of Excellence in Advanced Quantum Sensing under Army Research Office grant number W911NF202076, ONR grant number N00014-19-1-2181, and the U.S. Department of Energy, Office of Science, National Quantum Information Science Research Centers, Superconducting Quantum Materials and Systems Center (SQMS) under contract number DE-AC02-07CH11359.

---

<sup>1</sup> Overstreet, C., Asenbaum, P., Kovachy, T., Notermans, R., Hogan, J. M., & Kasevich, M. A. (2018). Effective inertial frame in an atom interferometric test of the equivalence principle. *Physical review letters*, 120(18), 183604.

<sup>2</sup> Asenbaum, P., Overstreet, C., Kim, M., Curti, J., & Kasevich, M. A. (2020). Atom-interferometric test of the equivalence principle at the 10– 12 level. *Physical Review Letters*, 125(19), 191101.

<sup>3</sup> Fray, S., Diez, C. A., Hänsch, T. W., & Weitz, M. (2004). Atomic interferometer with amplitude gratings of light and its applications to atom based tests of the equivalence principle. *Physical Review Letters*, 93(24), 240404.

<sup>4</sup> Bonnin, A., Zahzam, N., Bidel, Y., & Bresson, A. (2013). Simultaneous dual-species matter-wave accelerometer. *Physical Review A*, 88(4), 043615.

<sup>5</sup> Schlippenbauer, D., Hartwig, J., Albers, H., Richardson, L. L., Schubert, C., Roura, A., ... & Rasel, E. M. (2014). Quantum test of the universality of free fall. *Physical Review Letters*, 112(20), 203002.

<sup>6</sup> Tarallo, M. G., Mazzoni, T., Poli, N., Sutyrin, D. V., Zhang, X., & Tino, G. M. (2014). Test of Einstein equivalence principle for 0-spin and half-integer-spin atoms: search for spin-gravity coupling effects. *Physical review letters*, 113(2), 023005.

<sup>7</sup> Zhou, L., Long, S., Tang, B., Chen, X., Gao, F., Peng, W., ... & Zhan, M. (2015). Test of equivalence principle at 1 0– 8 level by a dual-species double-diffraction Raman atom interferometer. *Physical review letters*, 115(1), 013004.

<sup>8</sup> Barrett, B., Antoni-Micollier, L., Chichet, L., Battelier, B., Léveillé, T., Landragin, A., & Bouyer, P. (2016). Dual matter-wave inertial sensors in weightlessness. *Nature communications*, 7(1), 1-9.

<sup>9</sup> Kuhn, C. C. N., McDonald, G. D., Hardman, K. S., Bennetts, S., Everitt, P. J., Altin, P. A., ... & Robins, N. P. (2014). A Bose-condensed, simultaneous dual-species Mach–Zehnder atom interferometer. *New Journal of Physics*, 16(7), 073035.

<sup>10</sup> Rosi, G., D’Amico, G., Cacciapuoti, L., Sorrentino, F., Prevedelli, M., Zych, M., ... & Tino, G. M. (2017). Quantum test of the equivalence principle for atoms in coherent superposition of internal energy states. *Nature communications*, 8(1), 1-6.

<sup>11</sup> Graham, P. W., Kaplan, D. E., Mardon, J., Rajendran, S., & Terrano, W. A. (2016). Dark matter direct detection with accelerometers. *Physical Review D*, 93(7), 075029.

<sup>12</sup> Abe, M., Adamson, P., Borcean, M., Bortoletto, D., Bridges, K., Carman, S. P., ... & Wilkason, T. (2021). Matter-wave atomic gradiometer interferometric sensor (MAGIS-100). *Quantum Science and Technology*, 6(4), 044003.

<sup>13</sup> Li, J., RM da Silva, G., Huang, W. C., Fouda, M., Bonacum, J., Kovachy, T., & Shahriar, S. M. (2021). High sensitivity multi-axes rotation sensing using large momentum transfer point source atom interferometry. *Atoms*, 9(3), 51.

<sup>14</sup> McGuirk, J. M., Snadden, M. J., & Kasevich, M. A. (2000). Large area light-pulse atom interferometry. *Physical review letters*, 85(21), 4498.

<sup>15</sup> Kotru, K., Butts, D. L., Kinast, J. M., & Stoner, R. E. (2015). Large-area atom interferometry with frequency-swept Raman adiabatic passage. *Physical review letters*, 115(10), 103001.

<sup>16</sup> Kovachy, T., Asenbaum, P., Overstreet, C., Donnelly, C. A., Dickerson, S. M., Sugarbaker, A., ... & Kasevich, M. A. (2015). Quantum superposition at the half-metre scale. *Nature*, 528(7583), 530-533.

<sup>17</sup> Kitagawa, M., & Ueda, M. (1993). Squeezed spin states. *Physical Review A*, 47(6), 5138.

---

<sup>18</sup> Schleier-Smith, M. H., Leroux, I. D., & Vuletić, V. (2010). Squeezing the collective spin of a dilute atomic ensemble by cavity feedback. *Physical Review A*, 81(2), 021804.

<sup>19</sup> Leroux, I. D., Schleier-Smith, M. H., & Vuletić, V. (2010). Implementation of cavity squeezing of a collective atomic spin. *Physical Review Letters*, 104(7), 073602.

<sup>20</sup> Zhang, Y. L., Zou, C. L., Zou, X. B., Jiang, L., & Guo, G. C. (2015). Detuning-enhanced cavity spin squeezing. *Physical Review A*, 91(3), 033625.

<sup>21</sup> Sørensen, A. S., & Mølmer, K. (2002). Entangling atoms in bad cavities. *Physical Review A*, 66(2), 022314.

<sup>22</sup> Li, J., da Silva, G. R., Kain, S., & Shahriar, S. M. (2022). A generalized echo squeezing protocol with near-Heisenberg limit sensitivity and strong robustness against excess noise and variation in squeezing parameter. *arXiv preprint arXiv:2204.08681*.

<sup>23</sup> Sarkar, R., Fang, R., & Shahriar, S. M. (2018). High-Compton-frequency, parity-independent, mesoscopic Schrödinger-cat-state atom interferometer with Heisenberg-limited sensitivity. *Physical Review A*, 98(1), 013636.

<sup>24</sup> Fang, R., Sarkar, R., & Shahriar, S. M. (2020). Enhancing the sensitivity of an atom interferometer to the Heisenberg limit using increased quantum noise. *JOSA B*, 37(7), 1974-1986.

<sup>25</sup> Davis, E., Bentsen, G., & Schleier-Smith, M. (2016). Approaching the Heisenberg limit without single-particle detection. *Physical review letters*, 116(5), 053601.

<sup>26</sup> Hosten, O., Krishnakumar, R., Engelsen, N. J., & Kasevich, M. A. (2016). Quantum phase magnification. *Science*, 352(6293), 1552-1555.

<sup>27</sup> Salvi, L., Poli, N., Vuletić, V., & Tino, G. M. (2018). Squeezing on momentum states for atom interferometry. *Physical review letters*, 120(3), 033601.